Adsorption 11: 443–447, 2005

Adsorbate Transport in Nanopores

SURESH K. BHATIA*, OWEN G. JEPPS AND DAVID NICHOLSON
Division of Chemical Engineering, The University of Queensland, Brisbane QLD 4072, Australia
sureshb@cheque.uq.edu.au

Abstract. We present a tractable theory of transport of simple fluids in cylindrical nanopores, considering trajectories of molecules between diffuse wall collisions at low-density, and including viscous flow contributions at higher densities. The model is validated through molecular dynamics simulations of supercritical methane transport, over a wide range of conditions. We find excellent agreement between model and simulation at low to medium densities. However, at high densities the model tends to over-predict the transport behaviour, due to a large decrease in surface slip that is not well represented by the model. It is also seen that the concept of activated diffusion, commonly associated with diffusion in small pores, is fundamentally invalid for smooth pores.

Keywords: transport phenomena, diffusion, nanopores, statistical mechanics, slip flow

Introduction

The problem of transport in confined spaces is one of long-standing interest, now receiving renewed attention due to its importance to the numerous applications of new materials. The history of the subject dates back to the seminal work of Knudsen (1909) and Smoluchowski (1910), subsequently extended to include the effect of intermolecular collisions (Pollard et al., 1948). Nevertheless, despite this long history, our understanding of the subject is still relatively rudimentary. Efforts to incorporate more realistic interactions have had limited success, with mechanical models fast becoming intractable. It is therefore still common to empirically treat the transport as activated, and the validity of such procedures is unclear. In larger pores the 'dusty gas' model (Mason, 1967) superposes diffusive and viscous flow contributions to give an overall diffusion coefficient

$$D_t = \left(D_o + \frac{r_p^2 \hat{\rho} k_B T}{8\eta} \right) \left(\frac{\partial \ln(f)}{\partial \ln(\hat{\rho})} \right)_T \qquad (1)$$

The Poiseuille viscous term in Eq. (1) assumes that the density profile is homogeneous, which is inaccurate in microporous transport. Work in our laboratory (Bhatia et al., 2003a,b) has refined a recent viscous model for strongly inhomogeneous transport (Bitsanis et al., 1988), introducing a slip condition to reflect the non-vanishing transport coefficient observed at low densities, and assuming that the chemical potential (rather than the pressure) is constant across the pore cross-section. These refinements yield a density-dependent transport coefficient

$$D_{\rm to}(\hat{\rho}) = \frac{2k_B T}{\hat{\rho} r_p^2} \left[\frac{1}{k r_o \rho(r_o)} \left(\int_0^{r_o} r\rho(r)\, dr \right)^2 + \int_0^{r_o} \frac{dr}{r\eta(\bar{\rho}(r))} \left(\int_0^{r} r'\rho(r')\, dr' \right)^2 \right] \qquad (2)$$

for temperature T, Boltzmann's constant $k_{\rm B}$, local density ρ, locally-averaged density $\bar{\rho}$, viscosity η, mean pore density $\hat{\rho}$, radius at the potential minimum $r_{\rm o}$, and pore radius r_p, and wall collision rate k. The viscosity is determined based on the locally averaged density. We identify diffusive and viscous terms (the first and second terms in the square brackets), consistent with the dusty gas approach. Comparison of the predictions of Eq. (2) with computer simulation showed satisfactory agreement, with the diffusive term less reliable at low densities.

*To whom correspondence should be addressed.

At low densities, fluid-fluid interactions (and thus the viscosity) become negligible, and one can develop a transport theory based on molecule trajectories in the absence of collisions. In this paper we present such a theory, and show that it gives excellent agreement with simulation results in the low-density limit. At higher densities, a combination of the density-dependent viscous term from Eq. (2) and the low-density transport coefficient provides an accurate model over a wide range of pore sizes, temperatures and densities, when compared with simulation.

Transport Models

We first develop a low-density limit theory for microporous transport of simple fluids along a cylindrical pore. We consider a particle moving under the influence of the solid-fluid potential $\phi_{\rm fs}(r)$, and a constant external axial force Γ_z. In this field, the particle will oscillate across the pore as it accelerates along the pore. The molecule undergoes a diffuse reflection at the wall, losing all of its incident momentum on average. The transport coefficient is given by (Jepps et al., 2004)

$$D_{\rm to} = j_z k_{\rm B} T/\hat{\rho}\Gamma_z = k_{\rm B} T\langle u_z\rangle/\Gamma_z = k_{\rm B} T\langle\tau\rangle/m \quad (3)$$

for axial number flux j_z, total streaming velocity $\langle u_z\rangle$, and mean oscillation time between wall reflections $\langle\tau\rangle$. To determine the oscillation time for an arbitrary trajectory we determine the dynamics using the Hamiltonian

$$H = \phi_{fs}(r) + p_r^2/2m + p_\theta^2/2mr^2 + p_z^2/2m - \Gamma_z z \quad (4)$$

Using Hamiltonian dynamics, the oscillation time can be determined to be (Jepps et al., 2004)

$$\tau(r,\, p_r,\, p_\theta) = 2m\int_{r_{co}(r,p_r,p_\theta)}^{r_{c1}(r,p_r,p_\theta)} \left\{2m[\phi_{fs}(r) - \phi_{fs}(r')] + p_r^2(r) + \frac{p_\theta^2}{r^2}\left(1 - \frac{r^2}{r'^2}\right)\right\}^{-1/2} dr' \quad (5)$$

where $r_{c1}(r,\, p_r,\, p_\theta)$ and $r_{co}(r,\, p_r,\, p_\theta)$ are the values of r' corresponding to the solution of $p_r(r', r,\, p_r,\, p_\theta) = 0$. If we assume a canonical distribution for non-axial components, then we predict a low-density limit transport coefficient

$$D_{\rm to}^{\rm LD} = \frac{2}{\pi m\int_0^\infty re^{-\beta\phi_{fs}(r)}dr}\int_0^\infty e^{-\beta\phi_{fs}(r)}dr \times\int_0^\infty e^{-\beta p_r^2/2m}dp_r\int_0^\infty e^{-\beta p_\theta^2/2mr^2}dp_\theta \times\int_{r_{co}(r,p_r,p_\theta)}^{r_{c1}(r,p_r,p_\theta)}\frac{dr'}{p_r(r', r,\, p_r,\, p_\theta)},\quad \beta = (kT)^{-1}. \quad (6)$$

Equation (6) is consistent with the Knudsen result (Knudsen, 1910)—on substituting $\phi_{fs}(r) \equiv 0$ into (6), one obtains

$$D_{\rm to}^{\rm LD} = \sqrt{32r_{ph}^2 k_{\rm B} T/9\pi m}. \quad (7)$$

with hard-wall pore radius $r_{\rm ph}$. As discussed above, we adopt an alternative density-dependent model in which $D_{\rm to}^{\rm LD}$ represents the surface slip term in a viscous flow model, leading to the expression

$$D_{to}(\hat{\rho}) = D_{to}^{LD} + \frac{2k_{\rm B}T}{\hat{\rho}r_p^2}\int_0^{r_o}\frac{dr}{r\eta(\bar{\rho}(r))} \times\left(\int_0^r r'\rho(r')\,dr'\right)^2. \quad (8)$$

Model System and Simulation Methods

Equation (6) has been solved to obtain estimates of the transport diffusion coefficient for methane adsorption in silica cylindrical pores. These estimates were compared with data collated from equilibrium and nonequilibrium molecular dynamics (EMD and NEMD respectively) simulations. In both cases, the silica cylindrical pore walls were modelled as infinitely thick layers of close-packed LJ sites having (Bhatia et al., 2003a, 2003b) $\varepsilon_s/k_{\rm B} = 290$ K, $\sigma_s = 0.29$ nm. Methane was modelled as an LJ atom with $\varepsilon_f/k_{\rm B} = 148.1$ K, $\sigma_f = 0.381$ nm. The solid-fluid interaction was determined using Lorentz-Berthelot combining rules, with $\phi_{fs}(r)$ determined as an axial and angular average. Reflections between molecules and the pore wall are treated using diffuse boundary conditions (Cracknell et al., 1995). Density information and initial conditions were obtained from Grand-Canonical Monte Carlo (GCMC) simulations. During MD runs, a Gaussian thermostat (Evans et al., 1990) was applied to maintain constant temperature. Each simulation contained at least 500 molecules, and lasted 10^7 steps.

In EMD the transport coefficient was obtained from the autocorrelation of the instantaneous axial fluid streaming velocity (fluctuating from the diffuse reflections) via the Green-Kubo relation (Nicholson et al., 2000).

$$D_{to} = N \lim_{\tau\to\infty} \int_0^\tau \langle u_z(0)u_z(t)\rangle \, dt \tag{9}$$

In NEMD a constant axial acceleration in the range of 0.001–0.02 nm/ps^2 was applied to fluid particles, and a transport coefficient computed from Eq. (3), using the axial number flux and the mean fluid number density.

Results and Discussion

Supercritical Isotherms

We determined the isotherms at five different temperatures in the range 300–500 K, and at various pore sizes. The transport is single-file up to a radius of approximately 1.05 nm, where the solid-fluid potential minimum moves away from the pore centre. We find a linear (i.e. Henry's law) region up to a methane pore density of approximately 1 nm^{-3}. Saturation is not achieved even at high fugacity exceeding 100 bar. Nevertheless, a pore-size dependent capacity is observed, with the largest pore size having the highest capacity, which may be attributed to the effect of intermolecular interactions.

Low-Density Transport

Figure 1(a) depicts the variation of the transport coefficient of methane with pore diameter at 450 K in the Henry law region, obtained from simulation and from Eq. (6). The MD results represent an average taken over 6–10 runs at fluid densities below 0.5 nm^{-3}, with error bars depicting the standard deviation. We observe excellent agreement between EMD, NEMD, and the theory, even in the 0.75 nm pore in which only single file diffusion can occur. It is clear, however, that the Knudsen limit is not a good approximation—whether the effective hard-wall radius is set to the actual pore radius (dashed-dotted line in Fig. 1(a)), or a position corresponding to the first layer of fluid molecules (dashed line in Fig. 1(a)).

We also compare the axial streaming velocity profiles obtained from simulation with those predicted by the theory, obtained from Eq. (6):

$$\langle u_z(r)\rangle = \frac{2\Gamma_z}{\pi m r k_B T} \int_0^\infty e^{-\beta p_r^2/2m} dp_r \times \int_o^\infty e^{-\beta p_\theta^2/2mr^2} dp_\theta \times \int_{r_{co}(r,p_r,p_\theta)}^{r_{c1}(r,p_r,p_\theta)} \frac{dr'}{p_r(r', r, p_r, p_\theta)} \tag{10}$$

Comparison of velocity profiles predicted by Eq. (10) with simulation results gave excellent agreement in all cases. Figure 1(b) depicts the agreement for a 2.39 nm pore at 450 K, with an applied acceleration of 0.015 nm/ps^2.

Microporous transport is commonly analysed in terms of an activated diffusion model. From our theory, an activation energy can be determined by the relation

$$E = -\, d \ln D_{\text{to}}^{\text{LD}} / d\beta = \langle (H - p_{z0}^2/2m)\tau \rangle / \langle \tau \rangle - \langle V(r) \rangle \tag{11}$$

The activation energy predicted by the theory is compared with the minimum potential energy in the pore in

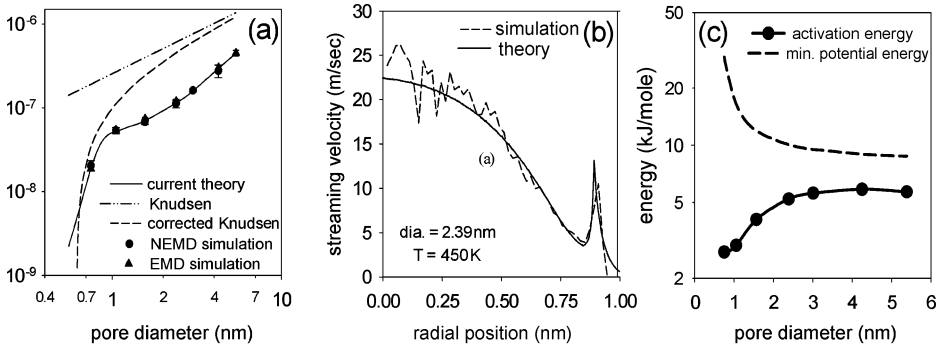

Figure 1. Results for low-density limit model—(a) comparison of transport coefficient from theory and simulation; (b) comparison of velocity profile from theory and simulation; (c) examination of hypothesised activated transport model.

Fig. 1(c). While it is common to assume some relation of the form $E = a|\phi_{\min}|$, $0.3 < a < 1$, it is clear from Fig. 1(c) that such an assumption is unreliable, and that the activation energy is instead related to the excess of the suitably averaged Hamiltonian over the mean potential energy, representing a temperature-dependent potential barrier.

Density-Dependent Model

The density variation of the transport coefficient at 450 K was computed for various pore sizes, in order to test the adequacy of the expression in Eq. (8), and to compare it with its predecessor, Eq. (2). Values of the transport coefficient were obtained from EMD and NEMD simulations, and compared with the predictions from Eqs. (2) and (8) using the GCMC density profile. These comparisons appear in Fig. 2.

Consistent with our earlier work for mesopores (Bhatia et al., 2003a, 2003b) and that of others (Arya et al., 2001; Nicholson, 2002), there is good agreement between the EMD and NEMD values of the coefficient, confirming their equivalence in the micropore region. As seen in the Fig. 2, the calculations based on Eq. (8) can represent the density variation of the transport coefficient very well up to the maximum, but the subsequent decline is somewhat less steep. This is largely because use of the Henry's law transport coefficient in the first term on the right hand side overlooks the decline in oscillation period due to intermolecular interactions at high density. Use of this term neglects the density-dependence in the nature of the solid-fluid momentum exchange, which may be significant at higher densities. Nevertheless, it is evident that the new approach is a considerable improvement over the earlier one in Eq. (2), given by the dashed curves in Fig. 2, which underpredicts the Henry's law transport coefficient. Qualitatively similar results were obtained at the other temperatures observed, and in the other pore sizes.

A further feature of the dashed curves in Fig. 2 is that at the smallest diameter of 0.75 nm, where the potential minimum is at the pore centre (and transport is in single file), Eq. (2) incorrectly yields a vanishing transport coefficient. On the other hand Eq. (8) accurately predicts the behaviour with a vanishing viscous part due to the absence of particle crossing. The density variation of the transport coefficient is predominantly due to viscous effects, which are virtually absent in single file diffusion. For single file diffusion, the effect of intermolecular interactions on the collective transport coefficient is negligible—the interaction force is essentially axial so that the oscillation motion, and therefore the centre-of-mass motion, is unaffected. Consequently the transport diffusivity is independent of density, as confirmed in Fig. 2(a).

The classical nature of the transport diffusivity is evident in Fig. 3(a), showing the linearity of the mean squared displacement of the centre of mass with time, at long time, obtained from EMD at low (8×10^{-5} nm^{-3}) and high (3.84 nm^{-3}) density. However, using the mean squared displacement of individual molecules (Fig. 3(b)), the long-time slope is unity at low density but approaches 0.7 at high density, indicating transition to non-classical self-diffusion when intermolecular interactions become important. This anomalous $\langle z^2 \rangle \propto t^{1/2}$ self-diffusion is well-documented (Hahn et al., 1998; Sholl et al., 1997; Mon et al., 2002). However, the transport diffusivity remains consistent with the classical

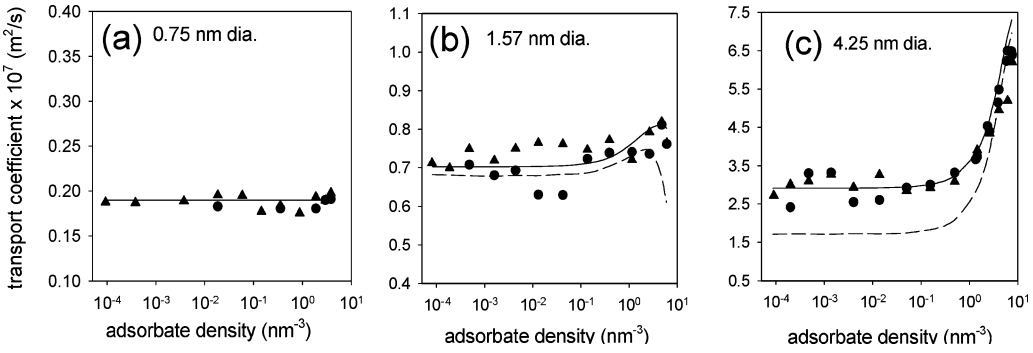

Figure 2. Transport coefficients obtained for methane in cylindrical silica pores of various radii at 450 K from the density-dependent models—Eq. (8) (solid line), Eq. (2) (dashed line)—and from simulation—EMD (triangles) and NEMD (circles).

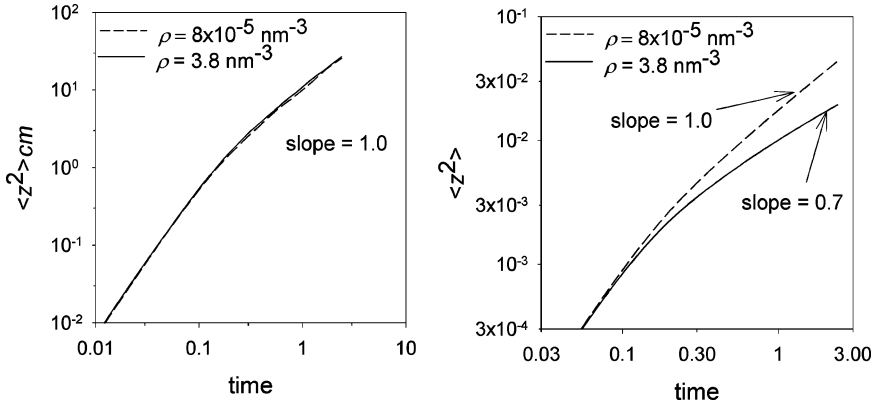

Figure 3. In single file diffusion, (a) the (collective) transport diffusion process obeys the Einstein relation, whereas (b) the self-diffusion process is observed to be anomalous at high densities.

Einstein relation, and the present theory is therefore still capable of predicting the correct transport diffusivity in this case.

Conclusions

We develop here a statistical mechanical low-density limit model of the microporous transport of simple fluids, considering the trajectories of molecules in the solid-fluid potential field. The principles of this approach can be applied to systems with more complex boundaries, albeit at increased computational burden, as well as to systems with partially diffuse reflections. Nevertheless, the success of the theory now obviates the need for MD calculations of transport coefficients in nanopores at low density, at least with partially diffusely reflecting walls. This approach eliminates the statistical noise inherent to MD simulations, reducing the CPU time required by several orders of magnitude, and has also been successfully applied in slit pore geometries (Jepps et al., 2003; Jepps et al., 2004). The theory also contradicts commonly used empirical representations relating activation energy to pore minimum potential energy.

At densities beyond the Henry's law region, intermolecular interactions can be conveniently incorporated into the theory through an additional viscous flow term, using the recently developed refinement (Bhatia et al., 2003a, 2003b) of the LADM. This approach provides accurate predictions of the transport coefficient over a wide range of densities. At very high bulk fugacity, however, transport coefficient values are overpredicted, due to the large reduction in oscillation period not represented by the theory. In most circumstances, these fugacities correspond to densities well beyond the scope of interest for common applications.

Acknowledgment

Support of this research by an ARC Large Grant is gratefully acknowledged.

References

Arya, G., H.-C. Chang, and E. Maginn, *J. Chem. Phys*., **115**, 8112 (2001).
Bhatia, S.K. and D. Nicholson, *Phys. Rev. Lett*., **90**, 016105 (2003a).
Bhatia, S.K. and D. Nicholson, *J. Chem. Phys*., **119**, 1719 (2003b).
Bitsanis, I., T.K. Vanderlick, M. Tirrell, and H.T. Davis, *J. Chem. Phys*., **89**, 3152 (1988).
Cracknell, R.F., D. Nicholson, and N. Quirke, *Phys. Rev. Lett*., **74**, 2463 (1995).
Evans, D.J. and G.P. Morriss, *Statistical Mechanics of Nonequilibrium Liquids*, Academic Press, London, 1990.
Hahn, K. and J. Kärger, *J. Phys Chem. B*., **102**, 5766 (1998).
Jepps, O.G., S.K. Bhatia, and D.J. Searles, *Phys. Rev. Lett*., **91**, 126102 (2003).
Jepps, O.G., S.K. Bhatia, and D.J. Searles, *J. Chem. Phys*., **120**, 5396 (2004).
Knudsen, M., *Ann. Phys. (Leipzig)*, **28**, 75 (1909).
Mason, E.A., A.P. Malinauskas, and R.B. Evans, *J.Chem.Phys*., **46**, 3199 (1967).
Mon, K.K. and J.K. Percus, *J. Chem. Phys*., **117**, 2289 (2002).
Nicholson, D. and K. Travis, *in Recent Advances in Gas Separation by Microporous Membranes*, N. Kanellopoulos (Ed.), Elsevier, Amsterdam, 2000.
Nicholson, D., *Mol. Phys.*, **100**, 2151 (2002).
Pollard, W.G. and R.D. Present. *Phys. Rev.*, **73**, 762 (1948).
Sholl, D.S. and K.A. Fichthorn, *Phys. Rev. E*, **55**, 7753 (1997).
von Smoluchowski, M., *Ann. Physik. (Leipzig)*, **33**, 1559 (1910).